2017

A Comparison of Industry Standard and New Consumer-Grade Particulate Matter Measurements, and Insights from Air Pollution Vectoring in Reno, Nevada

Samuel Taylor

Abstract

Instrumentation for the measurement of particulate matter (PM) in the atmosphere is an extensively researched topic. There are many instruments capable of quantifying ambient PM; however, these tend to be expensive and require intense maintenance. Recent developments in microcontrollers and a large movement to make instruments smaller and less expensive have resulted in the Plantower Technologies' PMS5003, for example. The device measures particulate matter in the atmosphere by counting and sizing aerosol by measurement of scattered light. It is small, inexpensive, and easily operated. It is necessary to compare this new instrument to some of the standard PM monitoring equipment used today. An experiment was setup to evaluate the PMS5003 against two BAM-1020s and two photoacoustic spectroscopy instruments, and it was discovered that the PMS5003 correlates well with the photoacoustic instruments. In addition, air pollution vectoring is also explored by coupling mass concentrations of PM obtained by the BAM-1020s and wind data obtained from an ultrasonic anemometer to explore the air pollution causes.

1 Introduction

Air pollution is a problem that has been discussed and researched for decades now, and it continues to be a hot topic even today. It impacts our daily lives on a scale that we don't completely appreciate sometimes. It affects our health, our weather, and our activities. Particulate matter (PM) plays an important role in this. The term PM broadly defines a certain type of air pollution; it refers to all particles that are typically smaller than about ten microns in size, with different naming conventions for different sizes. (Chung et al., 2001) Being able to

accurately measure PM is crucial to understanding health risks for populations, and PM is closely monitored by the EPA in the USA.

With the recent widespread use and success of opensource microcontrollers like Arduino and Raspberry-Pi, creating scientific instruments has never been easier, cheaper, or more accessible. As a result, many people have taken to creating their own instruments or using this technology to crowdsource scientific data and research. This trend has been loosely dubbed as "Citizen Science," and represents significant opportunities for widespread data gathering. (Nature Publishing Group, 2015) PM measuring is not exempt from this. With the rise of these new, economical instruments, a new question needs to be answered: "How do microcontroller-based instruments compare to EPA-grade measurement devices?" This study aims to compare the Plantower PMS5003 to the EPA standard Beta Attenuation Monitor (BAM) and to photoacoustic spectroscopy (PAS) instruments.

Additionally, when air pollution data is combined with wind data, it is feasible to create "pollution roses." Using data gathered by an ultrasonic anemometer and the BAM-1020 units, local pollution source vectoring becomes possible. An air pollution rose combines pollution magnitude with wind direction to determine the direction from which large amounts of pollution are being transported. (Carslaw, 2017) By creating air pollution roses using data from days of high PM concentration in the air, the PM can be vectored, and a source direction can be determined. By using different types of collected PM data, it also becomes possible to make educated guesses about what is causing the air pollution.

2 Theory

2.1 BAM-1020 Operational Theory

Since the Clean Air Act amendments in 1999, beta attenuation monitoring has become a common technique for air quality monitoring in the United States. It was originally developed and utilized in the production of paper over 60 years ago; the method has since been revised for monitoring airborne particulate matter. (Gobeli et al., 2008)

Met One Instruments' BAM-1020s are stored indoors or inside an appropriate weatherproof container during operation. Each instrument has an inlet atop a pipe that extends through the roof of their enclosure. Depending on what the instrument is set up to measure, there are different inlet configurations. If a BAM-1020 capable of measuring PM10 (particulate matter ten microns or smaller in diameter) is desired, then a PM10 filter inlet is fitted to the top of the pipe. If PM2.5 (particulate matter two and a half microns or smaller in diameter) is the desired pollutant to measure, then a PM2.5 cyclone is fitted atop the pipe, with a PM10 filter inlet attached on top of that. When air is pulled through these filters and cyclones, the polluted air is filtered and the remaining particulate matter in the air is of the desired size. (EPA, 1999)

The BAM-1020 contains a mildly radioactive ^{14}C (carbon-14) source, which is constantly emitting a steady and measurable stream of high-energy electrons, known as beta rays. When interacting with matter of any type, these electrons either lose energy or are absorbed entirely by the matter. This process is known as beta ray attenuation, from which the instrument gets its name. (Gobeli et al., 2008) The instrument also contains a thin quartz filter tape, which the particulate matter is deposited on to. Beer's Law constitutes that the absorbance of these beta rays is proportionate to the concentrations of the species that is attenuating in the material. (EPA, 1999) In other words, as more mass is gathered on the filter, the intensity of the beta rays

measured by the sensor decreases at an exponential rate. This can be modeled with the following equation:

$$I = I_0 e^{-\mu x}$$

where I is the measured intensity of the beta ray in counts per unit time through the dirty filter, I_0 is the initial intensity measured through the clean filter, μ is the absorption cross section of the sample material in meters squared per kilogram, and x is the mass concentration of the sample in kilograms per meter squared. Because μ is a constant, then x can be solved for and the mass concentration can be calculated once I and I_0 are known. (Gobeli et al., 2008)

2.2 Photoacoustic Spectroscopy Theory

Photoacoustic spectroscopy instruments utilize lasers to measure air pollutants in situ. Aerosol-laden air is pumped into the resonator chamber and then bombarded by a modulated laser source. As the particles absorb the light from the laser, they heat and expand the air around them. This process generates a sound wave within the resonator chamber. Using very sensitive microphones to detect these sound waves, the aerosols can be counted and measured with a high degree of accuracy. (Lewis, Arnott, Moosmüller, & Wold, 2008; Moosmfiller et al., 1998)

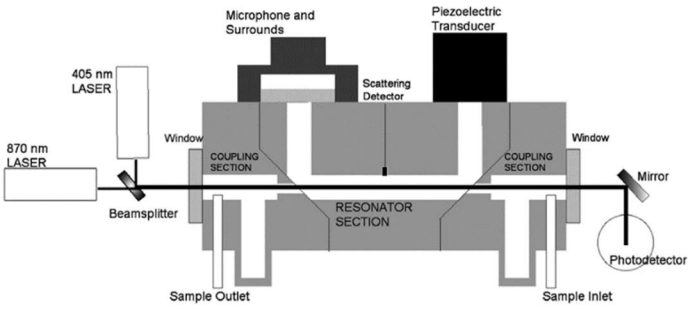

Figure 1: Diagram of the resonator chamber used in the dual wavelength photoacoustic spectroscopy instrument used in this experiment. The instrument operates at 405nm and 870nm. (Lewis, et al. 2008)

2.3 Plantower PMS5003 Operational Theory

The PMS5003 operates on the light scattering principle of Mie theory, which describes the scattering of light by a sphere. (Yong, Haoxin. 2016) This type of assumption is quite reasonable for dry areas, since moisture could cause particles to stick together, and thus skew measurements as the instrument attempts to quantify a non-homogenous sphere.

The instrument first intakes air through the front face by holes in its casing. The air is pulled across the main circuit board. When the air makes its way across the board, heavier particles much greater than PM10 are intended to fall out and collect on the board. This is crucial to the extended operation of the instrument, as it prevents the build up of material on the laser diode and photodiode located on the bottom of the instrument. (Yong, Haoxin. 2016) After the air passes over the board, it is then pulled through the holes in the circuit board to the measurement section. Here, the air passes through the measurement chamber. A laser diode irradiates the aerosol particles held in the air as it passes over the photodiode. The photodiode then intercepts the light scattered off the particles. Knowing the amount of light

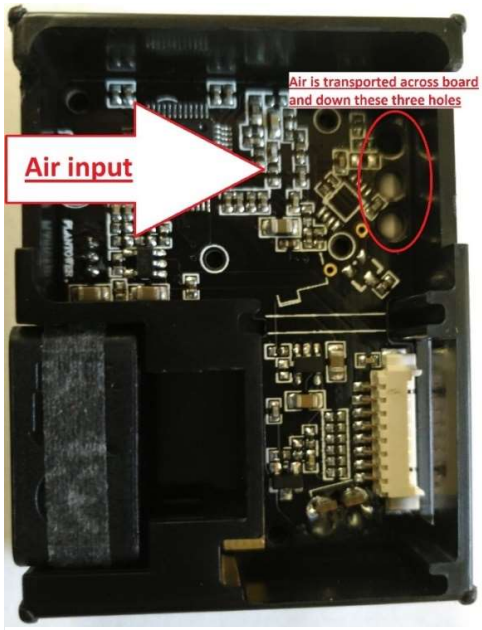

Figure 2: Internal image of the PMS5003. This is the top of the instrument. Air comes in through inlet holes, traverses the circuit board, then travels through three small holes to the measurement section of the instrument.

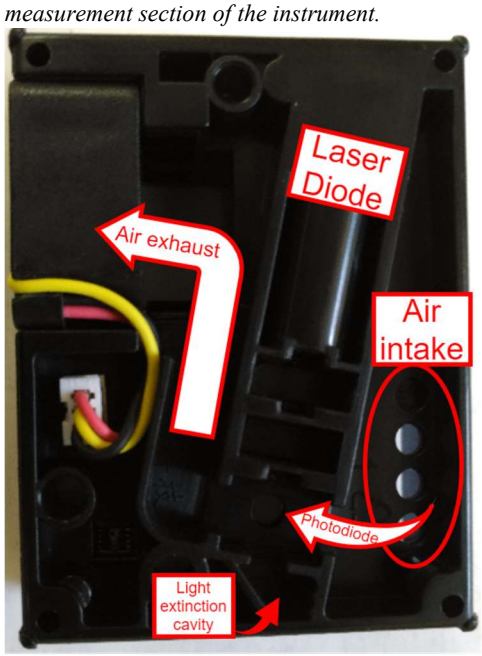

Figure 3: Internal image of the PMS5003. This is the bottom of the instrument. The air comes in through the intake holes and passes through the measurement section of the instrument.

that is scattered by the particles allows the instrument to calculate the diameters of the aerosols, as well as obtain a count of the particles. (Yong, Haoxin. 2016) This data is reported in mass concentrations. After the sample air is measured, it is then moved through the rest of the air channel and exhausted through the front of the instrument via a small fan. Figure 3 illustrates the measurement chamber of the instrument. Two laser collimators can be seen in front of the laser source, as well as a light extinction cavity. These two devices prevent stray light from interacting with the particles and skewing measurements.

2.4 Ultrasonic Anemometer Operational Theory

Ultrasonic anemometers are devices used to determine wind velocities in three dimensions through the properties of sounds waves. These devices are more accurate and have much higher time resolutions compared to mechanical anemometers. (Schotland, 1955) An ultrasonic anemometer operates by transmitting high frequency sounds through the air to a sensor. To obtain three dimensional readings of velocity, these instruments are typically fitted with multiple pairs of these sound emitters and sensors which are arranged in claw-like formations.

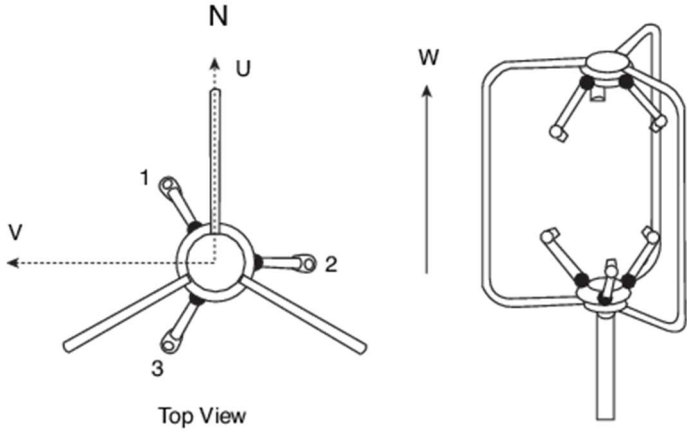

Figure 4: Illustration of the R.M. Young 81000 ultrasonic anemometer. Retrieved from: https://www.licor.com/env/help/eddypro6/Content/Resources/Images/Anemometer_Axes.png

Sound wave propagation is affected by several properties of the atmosphere, including water vapor and absolute temperature. This relationship is described by the following equation:

$$c = 20.067[T\left(1 + 0.319\frac{e}{p}\right)]^{\frac{1}{2}}$$

where c is the atmospheric speed of sound in meters per second, T is the temperature in degrees Kelvin, e is the water-vapor pressure, and p is the static pressure. (Schotland, 1955)

In addition, sound waves moving through the atmosphere are measurably affected by the wind. Wind disturbs the sound's movement, altering the spherical propagation of the sound wave. This effect is described by this equation:

$$(X - V_x t)^2 + (Y - V_y t)^2 + (Z - V_z t)^2 = (ct)^2$$

where X, Y, and Z are the coordinates of the origin of the sound wave, V_x,V_y, and V_z are the wind's velocity components, c is the speed of sound in the atmosphere, and t is the time the constant phase surface takes to reach the point indicated by X, Y, and Z. This equation can be simplified into three separate equations such that each component of the wind can be found individually and reported by the instrument. This is the reason why anemometers reporting wind data in three dimensions require three sets of sensors. (Schotland, 1995)

3 Data and Methods

3.1 Experiment Setup

The instruments utilized in this experiment include: two Met One Instruments BAM-1020s, two photoacoustic spectroscopy instruments, one Plantower Technologies PMS5003, and one R.M. Young Model 81000 Ultrasonic Anemometer.

For the instrument comparison, all PM monitoring instruments were setup to run atop the Leifson Physics building on the UNR campus. The BAMs were located inside of the

Figure 5: Experiment setup. Here, the instrument is attached to a BAM inlet pipe, where it was left to measure for the duration of the experiment.

observatory dome and the inlet pipes protruded through the dome. The BAMs were configured to run in PMcoarse mode. One BAM was setup to monitor PM10 and the other was setup to monitor PM2.5. These instruments were connected via an RS-232 data transfer cable, allowing them to communicate data and sync clocks.

The two photoacoustic instruments used were operating at two different laser frequencies. The first one operates with a 532-nanometer laser, while the second operates with a 405-nanometer laser. The air intake for these instruments is located on the west wall of the fourth floor of the building.

The PMS5003 was mounted inside of a metal box that was covered around the outside with Mylar bubble-wrap to prevent overheating. The bottom of this box was left open for air flow. An APC-220 radio was used to transmit data from outside to a Teensy 3.6 microcontroller on the inside of the building. The Teensy recorded all transmitted data to an SD card.

The ultrasonic anemometer was mounted atop a tripod on the roof of the Leifson Physics. The anemometer was oriented so that it faced north. This allowed for the anemometer to collect directional data correctly and no rotational algorithms needed to be applied to the data.

All data used in the comparison of the instruments was collected from September 19, 2017, to November 3, 2017. Anemometer data was collected from May 24, 2017, to November 3, 2017.

3.2 Explanation of PM Vectoring Method

Creating air pollution roses is very similar to creating wind roses. Like a wind rose, a pollution rose is a circular chart on which binned vectors are graphed. (Carslaw, 2017) The direction bins are typically in increments of about thirty degrees, though this varies depending on the desired resolution of direction. Different colors correspond to different magnitudes in either wind speed or air pollution. The length of the vector rendered onto the chart is reliant on the number of vectors that are put into that directional bin. On a wind rose, this makes it easy to see which direction the prevailing wind is coming from, along with which directions the largest wind speeds occur from. When these concepts are applied to a pollution rose, it makes it very easy to tell which direction the most significant air pollution is coming from. (Carslaw, 2017)

4 Results

Following the collection of the data via the experiment methods described in the previous section, the data was processed by performing various statistical analyses. Scatterplots and q-q plots are used to demonstrate correlation, while correlation tests were used to obtain Kendall and Pearson correlation values.

4.1 PMS5003 and BAM Comparisons

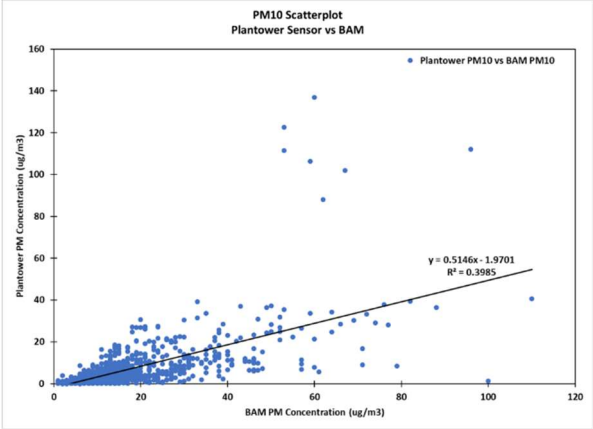

Figure 6: A scatterplot of PMS5003 PM10 against BAM PM10. Outliers heavily affect the correlation in this case.

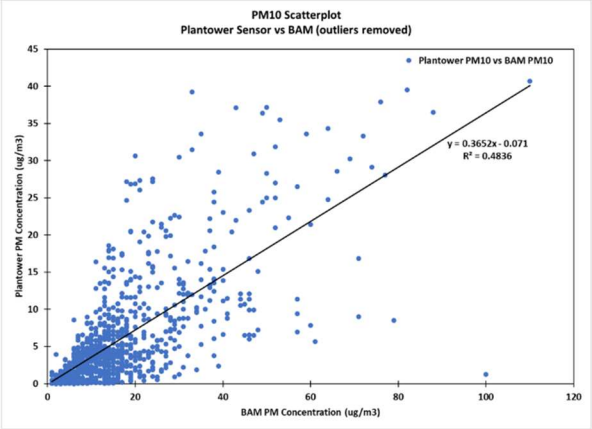

Figure 7: Another scatterplot of PMS5003 PM10 against BAM PM10. Outliers are removed here, resulting in a better correlation.

Figure 6 demonstrates the correlation between the BAM PM10 and the PMS5003 PM10. There is an obvious cluster of outliers that indicate the PMS5003 could have been overestimating the PM10 in comparison to the BAM. Due to the nature of these plots, it is difficult to determine if these resulted from measurement error or are indicative of a response in the instruments. Figure 7 shows the same scatterplot with the outlier cluster removed. This improved the R^2 value from 0.3985 to 0.4836. This is not a trivial increase of the correlation, though the scatterplot still shows the PMS5003 over and underestimating the PM10 consistently.

Figure 8 is the scatterplot of the PMS5003 PM2.5 against the BAM PM2.5. This scatterplot demonstrates a much higher correlation, with an R^2 value of 0.7882. The data seems to fall along a nice linear trend, though there is an offset of about 2.4 micrograms per meter cubed. The PMS5003

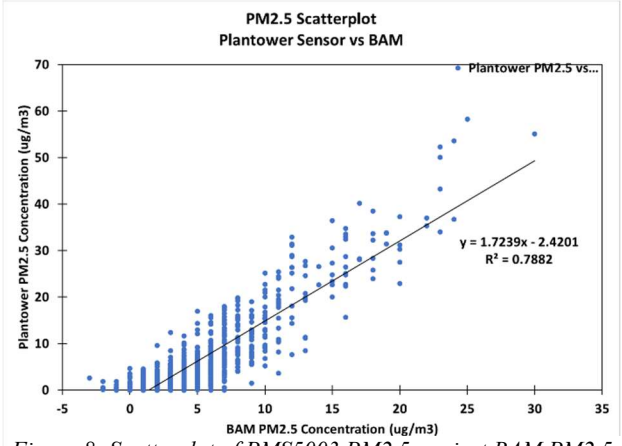

Figure 8: Scatterplot of PMS5003 PM2.5 against BAM PM2.5. Correlation is good, though PMS5003 tends to consistently over and under estimate the measurements.

also seems to both over and underestimate the PM2.5 in comparison to the BAM, much like with the PM10 comparison. However, this estimation error seems to be much less varied.

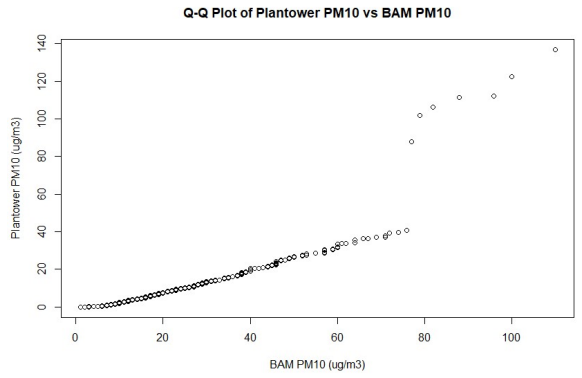

Figure 9: Q-Q plot of PMS5003 PM10 against BAM PM10. Outliers strongly affect this graph again. It seems that the PMS5003 consistently underestimates PM10 compared to the BAM.

Pearson: R = 0.6312309
Kendall: τ = 0.5264951

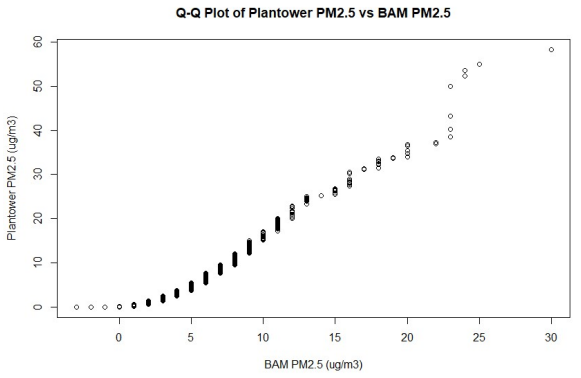

Figure 10: Q-Q plot of PMS5003 PM2.5 against BAM PM2.5. This graph suggests a better correlation, but PMS5003 underestimates BAM when concentrations are low and overestimates BAM when concentrations are high.

Pearson: R = 0.8878179
Kendall: τ = 0.6315592

Figure 9 shows the quantile-quantile (q-q) plot of the PMS5003 PM10 against the BAM PM10. Again, we can see the outliers from before strongly affecting the shape of the graph and the correlation values as a result. There is a nice linear trend in the data until the outliers occur, which strongly skews the graph. Upon examination of the axis, we can also see that the PMS5003 consistently underestimates the PM10 concentration in comparison to the BAM. With a Pearson correlation coefficient of 0.631 and Kendall correlation coefficient of 0.526, these instruments certainly correlate with one another to a degree, though further testing at higher concentrations of PM is needed.

Looking at figure 10, which displays the q-q plot of PMS5003 PM2.5 against BAM PM2.5, there seem to be a few outlier points as well, though not as extreme as in the PM10 comparison. The correlation is quite high for these instruments, considering their different air-intake methods

and their measurement processes. The PMS5003 appears to underestimate the BAM when PM2.5 concentrations are below about 15 micrograms per meter cubed, and it overestimates when concentrations are above the same mark. The offset of about 2.4 micrograms per meter cubed is also seen in this q-q plot near the origin of the chart. The Pearson coefficient of 0.888 is quite high and is exemplified by the way the data points fall along a somewhat linear trend. However, the Kendall coefficient of 0.632 conveys the over and under estimation problems illustrated in figure 8.

4.2 Photoacoustic Instrument Comparisons

The photoacoustic spectroscopy instruments report their data in the form of scattering and absorption coefficients. The scattering coefficient is what is necessary to calculate aerosol sizes. Because it was discovered that the PMS5003 and the photoacoustic spectroscopy instruments have a very high correlation, then the scattering coefficient given by the PAS instruments can be used to calculate particulate matter concentrations. This is done by using the slope of the linear regressions as mass scattering efficiency factors. This is described by the following equations:

$$\frac{1}{Mm} = \frac{1}{10^6 m}, \frac{ug}{m^3} = \frac{10^{-6} g}{m^3} \Rightarrow \frac{\frac{1}{10^6 m}}{\frac{10^{-6} g}{m^3}} = \frac{1}{10^6 m} \times \frac{m^3}{10^{-6} g} = \frac{m^2}{g}$$

The scattering coefficient is given in inverse megameters, which translates to 10^6 inverse meters. The mass concentrations are given in micrograms per meter cubed, which is 10^{-6} grams per meters cubed. Dividing the scattering coefficient by the mass concentration gives the mass scattering efficiency in meters squared per gram. This is the value obtained from the slope of the linear regression when a scattering coefficient is plotted against a mass concentration. Therefore, the scattering coefficient given by the PAS instruments can be divided by this mass scattering efficiency, resulting in the mass concentration. Doing this allows for easier

comparison of the instruments. Because the process only scales the values and does not change the shape of the graph, the correlation between the instruments is unchanged.

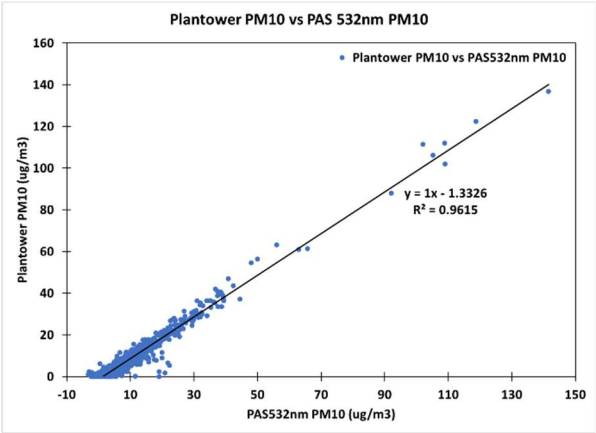

Figure 11: Scatterplot of PMS5003 PM10 against PAS 532nm calculated PM10. The correlation for these instruments is remarkably high.

Mass scattering efficiency factor for PAS 532nm Bsca to PM10: 1.3398 $\frac{m^2}{g}$

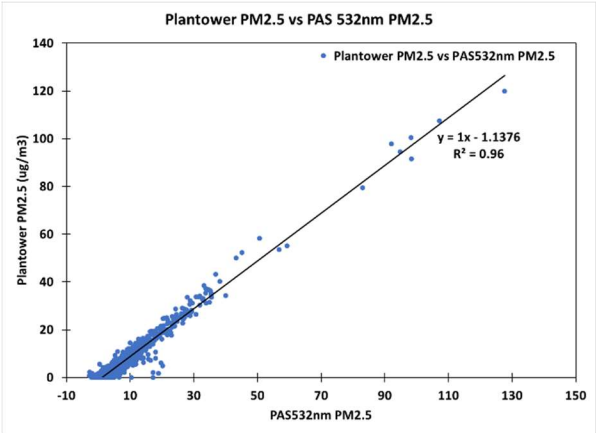

Figure 12: Scatterplot of PMS5003 PM2.5 against PAS 532nm calculated PM2.5. Again, the correlation is excellent, even better than the PM10.

Mass scattering efficiency factor for PAS 532nm Bsca to PM2.5: 1.485 $\frac{m^2}{g}$

Using the method described above, figures 11 and 12 were obtained. Both charts depict the calculated mass concentrations for two aerosol sizes, obtained from the 532nm photoacoustic instrument.

Figure 11 depicts the correlation between the PMS5003 PM10 and the PAS 532nm calculated PM10. These instruments obtain their data by similar measurement processes, which involves scattering light from a laser source off particles in the sampled air, which could be the reason these instruments demonstrate such a high linear correlation. The correlation at low concentration levels is high. However, there are very few data points gathered during high concentrations of PM in the atmosphere. The correlation pattern appears to hold at these higher densities, but further testing might reveal more.

In figure 12, a high correlation is demonstrated again. With an R^2 value of 0.96, the PMS5003 seems to measure PM2.5 most accurately. Again, we see high correlation at low mass concentrations, but it is difficult to tell for higher concentrations. It should also be noted that the mass scattering efficiency factor changes very little between the PM10 and PM2.5 calculations. Given the high correlation between the instruments at PM2.5, it can be hypothesized that this indicates the PMS5003 and the PAS 532nm instrument are attributing most of the ambient particulate matter to PM2.5.

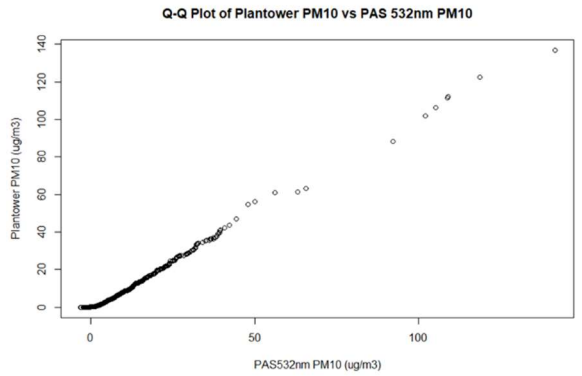

Figure 13: Q-Q plot of PMS5003 PM10 vs PAS 532nm calculated PM10. The plot really shows off the correlation for the distribution of values, though the PMS5003 may have correlation issues in higher mass concentrations.

Pearson: R = 0.9805674
Kendall: τ = 0.7669544

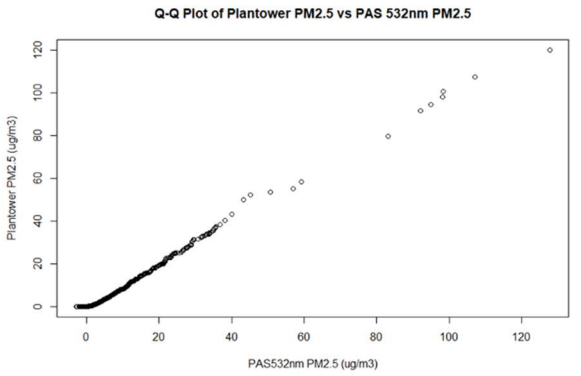

Figure 14: Q-Q plot of PMS5003 PM2.5 against PAS 532nm calculated PM2.5. Again, the correlation is very high at lower mass concentrations, but appears to suffer at higher concentrations.

Pearson: R = 0.9898887
Kendall: τ = 0.8490145

The q-q plot in figure 13 depicts the linear trend between the PMS5003 and the PAS 532nm instrument. The high correlation at lower mass concentrations is further reinforced by the Pearson coefficient of 0.98, while the questionable correlation during times of high mass concentration is also shown by the Kendall correlation of 0.767.

In figure 14, the same behavior can be seen, though with even higher correlation coefficients than before. The Pearson correlation is 0.989, which indicates that the PMS5003 has the highest

correlation when comparing PM2.5 concentrations for this PAS instrument. The higher Kendall coefficient of 0.849 confirms this further, showing how the data points deviate from the linear trend less.

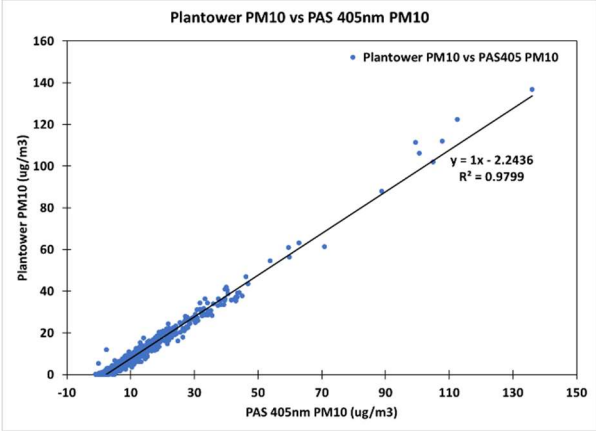

Figure 15: Scatterplot of PMS5003 PM10 against PAS 405nm calculated PM10. The correlations for the 405nm photoacoustic instrument are even higher than the 532nm instrument.

Mass scattering efficiency factor for PAS 405nmBsca to PM10: 2.3827 $\frac{m^2}{g}$

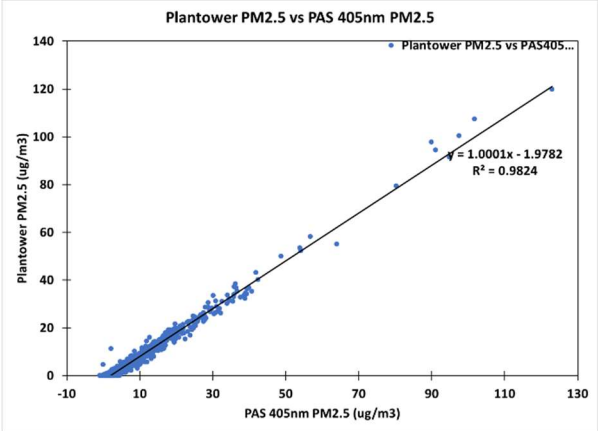

Figure 16: Scatterplot of PMS5003 PM2.5 against PAS 405nm calculated PM2.5. This is the highest correlation of all of the instruments.

Mass scattering efficiency factor for PAS 405nm Bsca to PM2.5: 2.6357 $\frac{m^2}{g}$

Figure 15 depicts the scatterplot of PMS5003 PM10 against the PAS 405nm instrument's calculated PM10. The R^2 for this scatterplot is higher than the PAS 532nm instrument's R^2 for its corresponding plot. As before, the linear trend at low concentrations is good, but deviations from the trend appear to occur more often at higher mass concentrations.

In figure 16, the R^2 is 0.982. This is the highest R^2 obtained from this experiment and further reinforces the previous theory that the PMS5003 achieves higher correlations for PM2.5 measurements. It should also be noted again that the mass scattering coefficients do not change much between the PM10 and PM2.5 calculations. This supports the hypothesis that the PMS5003 and the PAS instruments are attributing most ambient particulate matter to PM2.5.

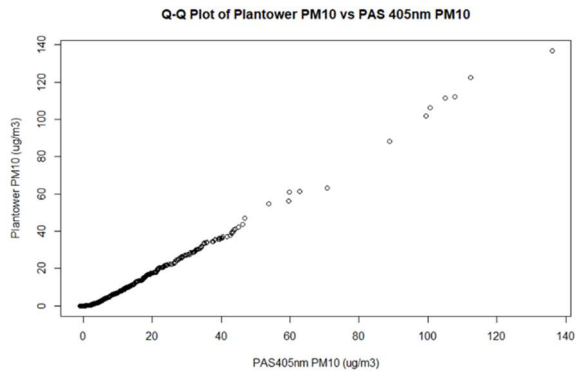

Figure 17: Q-Q plot of PMS5003 PM10 against PAS 405nm calculated PM10. The PMS5003 seems to best agree with the 405nm photoacoustic instrument, though higher concentrations need further investigation.

Pearson: R = 0.9797857
Kendall: τ = 0.7662629

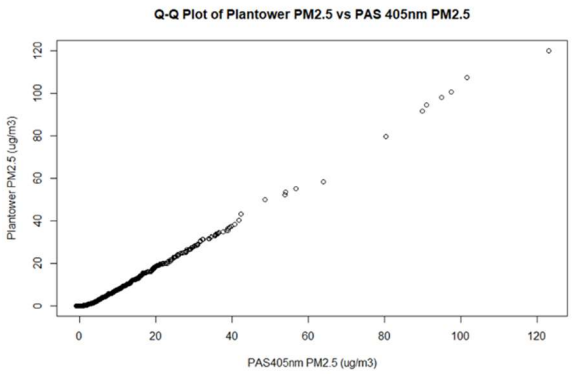

Figure 18: Q-Q plot of PMS5003 PM2.5 vs PAS 405nm calculated PM2.5. This correlation is nearly perfect. Again, high mass concentration values need to be investigated.

Pearson: R = 0.9911717
Kendall: τ = 0.8525781

Figure 17 is the q-q plot of the PMS5003 PM10 against the PAS 405nm instrument's calculated PM10. There appears to be a consistent pattern in these plots. The lower concentrations fit a linear trend the best, but high concentrations have larger deviations in values, which is always reflected in the lower Kendall correlation coefficients for these plots.

In figure 18, we see the same pattern again, though the deviations are less pronounced in the higher concentrations. This is reflected in the Kendall correlation coefficient. The q-q plot of the PMS5003 PM2.5 against the PAS 405nm instrument's calculated PM2.5 indicates the highest correlation yet, however. The Pearson coefficient of 0.991 is nearly perfect, further reinforcing confidence in this instrument's ability to measure ambient PM2.5.

4.3 PM Vectoring

Data used for the vectoring of particulate matter was BAM-1020 data taken in hourly increments and ultrasonic anemometer data averaged to hourly values to match the BAMs' time resolution. Using some code in R (Clifton, 2013), pollution roses were generated. In this

section, the process for utilizing a pollution rose to determine pollution source directions and pollution types will be discussed.

The first step is to find an air pollution event of interest. This can be done by observing the daily weather and sky conditions for pollution events, or by looking at a time series of collected air pollution data. Figure 20 displays the time series for pollution data from May 24, 2017 to November 3, 2017. There is a significant air pollution event around July 22. This event can be explored further through the use of air pollution roses.

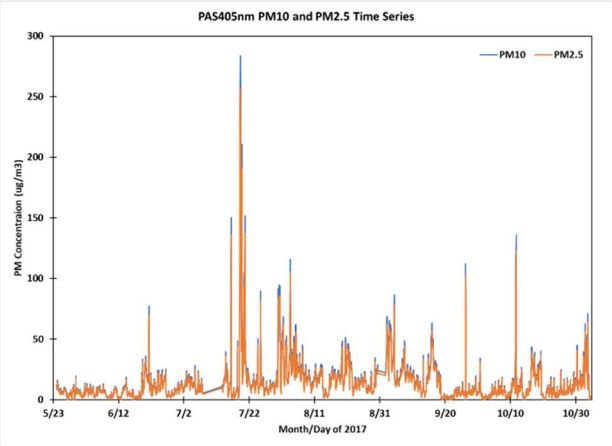

Figure 19: Time series of PAS405 calculated PM10 and PM2.5 concentrations from May 24 to November 3, 2017.

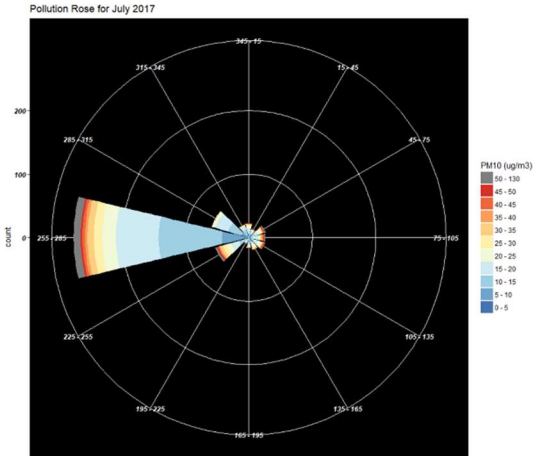

Figure 20: Air pollution rose for July 2017.

Figure 20 is the air pollution rose for the month of July. These can be a little hard to read when wind data from long periods of time are used, especially if the anemometer collecting the data is in a place where the prevailing wind for the area is very consistent (on top of a four-story building, for example). However, there is information to be gleaned from this chart. It appears that the prevailing wind direction on top of the Leifson physics building is westerly wind. This chart also shows that the air pollution is likely stemming from the west or southwest. The air pollution likely stayed in the air for a long period of time, as the other wind directions are also indicating high levels of pollution, but less consistently. This is likely caused by low wind speeds during the night hours, and high pollution levels being maintained during the pollution event.

The event can be visualized better if the data used to make the pollution rose is cut down to just the data from the pollution event. In figure 21, the day of July 19, 2017, sticks out as the most significant day in the air pollution event, and is likely the day that the pollution moved into Reno. From the graph, it is also possible to know the pollution type. PM10 values are high, but PM2.5 values are also high. Since PM10 includes PM2.5 within its size range, it can be concluded that this event mostly consists of PM2.5 in the atmosphere, and that there is actually very little PMcoarse (PM2.5 substracted out of PM10).

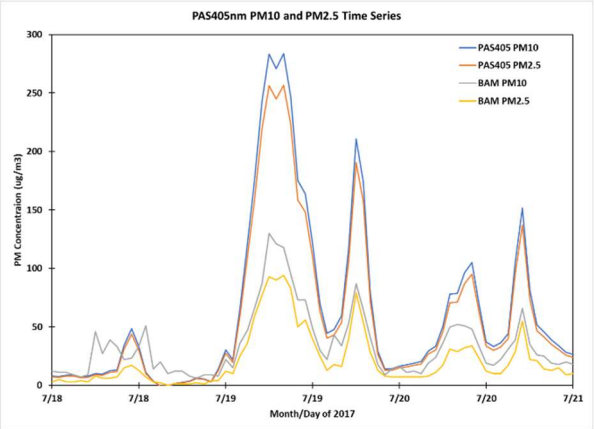

Figure 21:Time series of PM data from July 18 to July 21, 2017

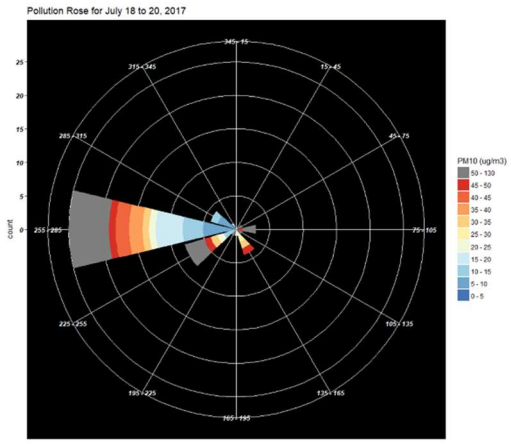

Figure 22: Air pollution rose for July 18 to July 20, 2017.

Figure 22 is the air pollution rose for the date in question. This plot makes it obvious that the strongest source of pollution is coming from the southwest, as the direction bins indicate very high pollution levels from those two directions. Because it consists primarily of PM2.5, and this data was collected during the summer in Reno, Nevada, we can conclude that this PM event was likely due to a fire in California. This hypothesis can be checked by looking at a visible satellite image of July 19, 2017.

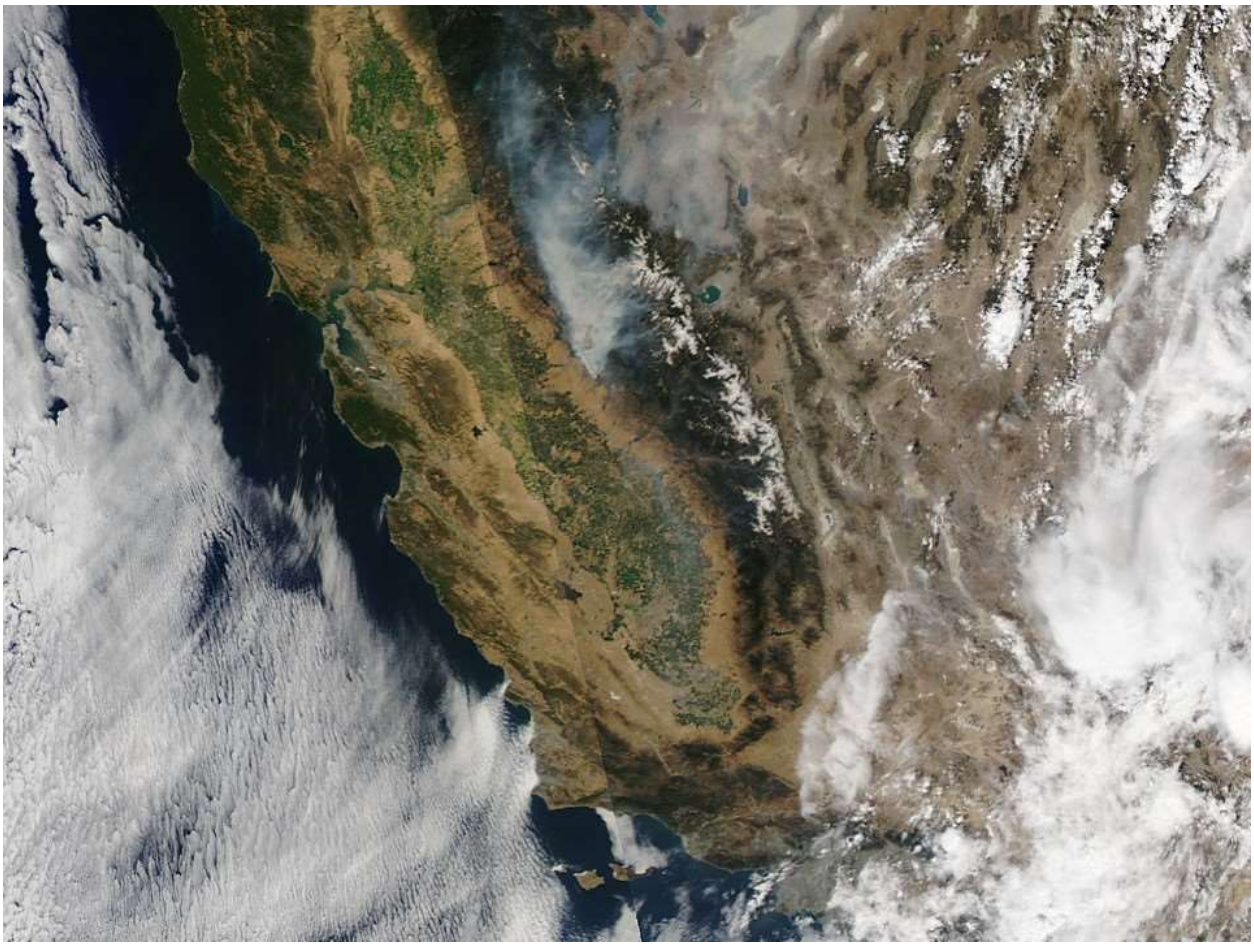

Figure 23: A visible satellite image of the west coast of the United States, taken by MODIS. Retreived from: https://lance-modis.eosdis.nasa.gov/imagery/subsets/?project=&subset=AERONET_Fresno&date=07%2F19%2F2017

Figure 23 confirms that a fire occurred in California around this time. Smoke was transported to Reno, Nevada, resulting in the air pollution levels shown in figures 19 and 21.

5 Conclusions

5.1 Instrument Comparison Conclusions

The PMS5003 is a remarkable instrument. It is inexpensive, small, and easy to use. Comparing this instrument to the Beta Attenuation Monitor, a decent correlation was found. It was shown that the PMS5003 tended to underestimate the BAMs PM10 consistently, though there was still a slight linear trend to the data. Removing outliers in the data improved this correlation, though some questions remain about the origin of those outliers. The PMS5003

correlated well with the BAM PM2.5. The scatterplot revealed an obvious linear trend, though the PMS5003 tended to both over and underestimate the BAM when measuring PM2.5.

It was discovered that the PMS5003 and the two photoacoustic spectroscopy instruments correlated very highly. The PAS 405nm instrument had the best correlations with the PMS5003, though the exact reason for this remains to be investigated. This is perhaps due to the wavelength of light that the instruments operate with. The laser diode in the PMS5003 needs to be investigated more. Both photoacoustic instrument comparisons showed a high correlation during times when particulate matter concentrations were low, while correlations during higher concentrations were more questionable, though still very reasonable.

The mass scattering efficiencies calculated for the photoacoustic instruments revealed that the PMS5003 and both photoacoustic instruments were attributing most particulate matter to the PM2.5 size. This was not corroborated by the BAM correlations, and needs to be considered.

5.2 PM Vectoring Conclusions

Air pollution roses and pollution vectoring can be very useful tools when looking into pollution problems and attempting to identify sources. Their usefulness alone is somewhat limited, but coupling them together with other data analysis methods, like time series and satellite images, can make them far more useful and interesting to use.

6 Future Work

Future work will include further testing of the PMS5003 against other particulate matter monitoring instruments in a burn chamber, among other conditions. Additionally, an instrument consisting solely of a Teensy 3.6 microcontroller, a PMS5003, and a GPS device is a desirable

apparatus with many uses that will be worked on. Such an instrument would make data collection and comparison easier to manage.

Additionally, an exploration of the uses for PM vectoring during local air pollution events should be investigated. Having multiple sites in a town for monitoring PM concentrations and wind data could prove useful for the triangulation of local pollution sources.

Acknowledgements

I'd like to thank Jayne Boehmler for her support on this project in helping me with ideas and offering suggestions on the direction of this paper. I'd also like to thank Dr. Patrick Arnott for allowing me the opportunity to work with and learn about these instruments over the past few years. Additionally, I would like to acknowledge my friends and family for supporting me through this endeavor, even while I secluded myself in a room to work into the small hours of the morning.

Bibliography

Chung, A., Chang, D. P. Y., Kleeman, M. J., Perry, K. D., Cahill, T. A., Dutcher, D., … Stroud, K. (2001). Comparison of Real-Time Instruments Used To Monitor Airborne Particulate Matter. *Journal of the Air & Waste Management Association*, *51*(1), 109–120. https://doi.org/10.1080/10473289.2001.10464254

Gobeli, D., Schloesser, H., & Pottberg, T. (2008). *Met One Instruments BAM-1020 Beta Attenuation Mass Monitor US-EPA PM2.5 Federal Equivalent Method Field Test Results*. *AWMA*. Retrieved from http://www.metone.com/docs/bam1020_whitepaper_2008a485awma.pdf

Lewis, K., Arnott, W. P., Moosmüller, H., & Wold, C. E. (2008). Strong spectral variation of biomass smoke light absorption and single scattering albedo observed with a novel dual-wavelength photoacoustic instrument. *Journal of Geophysical Research Atmospheres*, *113*(16). https://doi.org/10.1029/2007JD009699

Moosmfiller, H., Arnott, W. P., Rogers, C. F., Chow, J. C., Frazier, C. A., Sherman, L. E., & Dietrich, D. L. (1998). Photoacoustic and filter measurements related to aerosol light absorption during the Northern Front Range Air Quality Study (Colorado 1996/1997). *JOURNAL OF GEOPHYSICAL RESEARCH*, *103157*(20), 149–28. https://doi.org/10.1029/98JD02618

Schotland, R. M. (1955). The Measurement of Wind Velocity by Sonic Means. *Journal of Meteorology*. https://doi.org/10.1175/1520-0469(1955)012<0386:TMOWVB>2.0.CO;2

Clifton, Andy (2013). WindRose.R (Version 2.2) [Source code]. https://stackoverflow.com/questions/17266780/wind-rose-with-ggplot-r

(2015, August 18). Rise of the Citizen Scientist. *Nature News.* Nature Publishing Group. Retrieved from http://www.nature.com/news/rise-of-the-citizen-scientist-1.18192

Yong, Z., Haoxin, Z. (2016). Digital Universal Particle Concentration Sensor: PMS5003 Series Data Manual. *2016 Product Data Manual of PLANTOWER.* Retrieved from: http://www.patarnott.com/seniorthesis/pdf/plantower_pms5003_manual_v2_3.pdf

Carslaw, David C. (2017). Wind and Pollution Roses. *Openair Project.* Retrieved from: http://www.openair-project.org/examples/windpollutionroses.aspx